Dual Laser Study of Non-degenerate Two Wavelength Upconversion Demonstrated in Sensitizer-free $NaYF_4$:Pr Nanoparticles

Authors: Thomas J. de Prinse, Afshin Karami, Jillian E. Moffatt, Thomas B. Payten, Georgios Tsiminis, Lewis d S. Teixeira, Jingxiu Bi, Tak Kee, Elizaveta Klantsataya, Christopher J. Sumby, Nigel A. Spooner.

Thomas J. de Prinse*, Thomas B. Payten, Dr Jillian E. Moffatt, Dr Georgios Tsiminis, Lewis d S. Teixeira, Dr Elizaveta Klantsataya, Prof Nigel A. Spooner.
Institute for Photonics and Advanced Sensing (IPAS), School of Physical Sciences, The University of Adelaide, Adelaide, 5005, Australia.
E-mail: thomas.deprinse@adelaide.edu.au

Afshin Karami, Assoc. Prof Jingxiu Bi
School of Chemical Engineering, University of Adelaide, Adelaide, 5005, Australia

Thomas B. Payten, Dr Jillian E. Moffatt, Dr Georgios Tsiminis, Lewis d S. Teixeira, Prof Nigel A. Spooner
CRC for Optimising Resource Extraction, Kenmore, 4069, Australia.

Dr Georgios Tsiminis
ARC Centre of Excellence for Nanoscale BioPhotonics, The University of Adelaide, Adelaide, 5005, Australia.

Assoc. Prof Tak Kee, Prof Christopher J. Sumby,
Department of Chemistry, The University of Adelaide, Adelaide, 5005, Australia

Prof Nigel A. Spooner
Defence Science and Technology Group, Edinburgh, 5111, Australia.

Understanding the upconversion pathways of a rare-earth dopant is crucial to furthering the use of that material, either towards applications in imaging or elsewhere. This work outlines a new analysis approach that consists of using two synchronised widely-tuneable laser sources to explore the properties of upconverting materials. By examining sensitiser-free rare-earth nanoparticles based on a matrix of hexagonal sodium yttrium tetrafluoride (β-$NaYF_4$) doped with praseodymium but no ytterbium sensitiser, a 'non-degenerate' two-color upconversion fluorescence at a combined excitation of 1020 nm – 850 nm is shown. This

insight demonstrates the ability of this technique to locate and interrogate novel upconversion pathways. The dopant level of the nanoparticles could be modified without altering other factors, such as the particle's shape or size, that would also change optical properties and this allowed investigation of the dopant-level dependency of the optical properties. The approach also allows exploration of the time delay domain between the arrival time of the two non-degenerate excitation pulses, which allows modulation of the brightness from the visible light emissions. This work opens up the parameter space for the systematic synthesis and characterisation of new materials with non-degenerate upconversion emission.

Introduction

Rare-earth doped materials can produce luminescence emission at wavelengths shorter than those used to excite them, a process known as upconversion. [1] For this to occur in ions, the energies of two or more photons are combined, either with sequential absorption of photons or by energy transfer processes between neighbouring ions.[2] This collected energy is then released as one photon, which is blue shifted from the excitation wavelength. This effect has seen rare-earth dopants applied towards applications in sunlight harvesting,[3] high resolution imaging,[4] temperature sensing[5] and biological markers,[6] among many others.[7]

In order to understand the optical properties of rare-earth ions within a matrix, a suitable host material must be doped with the ion. Ideally, this host is a low phonon material, allowing for long excited-state lifetimes and higher quantum efficiencies.[8] Also, importantly, the dopant level should be able to be systematically altered without changing the physical properties of the material in unexpected ways.[9] In this regard, β-$NaYF_4$ nanoparticles can be used as a host for a single rare-earth dopant species. This single dopant level can be modified

easily during synthesis, with any changes to the optical properties resulting only from changes in the dopant ion interactions, as all other factors such as their morphology and crystal structure are shown to be controlled.[10]

Upconversion nanoparticles are usually designed to be excited by multiple photons of the same wavelength, such as excitation by one laser line in the near-infrared (NIR). This simplifies their use in many applications. An alternative approach is to utilise two sources of differing wavelength to excite a material, referred to here as 'dual non-degenerate' excitation. Dual non-degenerate excitation of nanoparticles has been demonstrated before, either to enhance a luminescence pathway[11] or to deplete an emission pathway.[4a, 12] Additionally, display technologies based on rare-earth dopants have been proposed that utilise two different NIR wavelengths for excitation, with visible light emitted most prominently at the overlap of the two beams.[13] These materials most commonly have a single pathway towards upconversion luminescence, often due to their dependence on a co-doped sensitizer ion such as ytterbium that gives rise to a specific energy transfer process between ions, in addition to absorption and energy transfer between the individual doped ion's intrinsic energy levels.

These more complex excitation and energy transfer pathways can only partially be explored with established upconversion characterisation techniques. To fully characterise the optical properties of rare-earth nanoparticles, two tuneable sources are required. In this work, a dual tuneable wavelength system has been built, capable of obtaining detailed excitation/emission profile maps over the visible and NIR range. Utilising the single ion-doped β-$NaYF_4$ matrix as a platform, in combination with the novel dual tuneable wavelength system, the properties

of the praseodymium(III) ion are studied at differing dopant levels, which elucidated a strong dual non-degenerate upconversion pathway.[14]

Results and Discussion

$NaYF_4$:Pr nanoparticles (NP) with 1, 2 and 5% doping of praseodymium were synthesised by the established thermal decomposition method.[15] To examine their morphology the materials were investigated by high-resolution TEM (HRTEM) imaging. HRTEM images for $NaYF_4$:Pr (1% Pr) are presented in **Figure 1** while the data for $NaYF_4$:Pr (2 and 5% Pr) are presented in **Figures 2S and 3S**, respectively. The HRTEM images confirm that particles with a hexagonal morphology are formed, consistent with the β-$NaYF_4$ structure for all three samples. The HRTEM images also reveal that synthesized NPs are uniformly-sized with mean particle sizes for $NaYF_4$:Pr (1% Pr) of 30 $\pm$ 3 nm (based on 80 NPs, Figure 1c). $NaYF_4$:Pr (2% Pr) and $NaYF_4$:Pr (5% Pr) were also uniformly-sized with mean particle sizes of 40 $\pm$ 6 nm and mean particle sizes of 27 $\pm$ 4 nm respectively (see supporting information). In all cases the interplanar distance of the synthesized NPs was measured to be approximately 0.52 nm (Figure 1a and supporting information), which corresponds to the interplanar distance of the (100) lattice plane for the hexagonal $NaYF_4$ structure (0.515 nm, JCPDS # 16-0334). The selected area electron diffraction (SAED) of synthesized $NaYF_4$:Pr NPs presented in Figure 1b and the supporting information also confirms a hexagonal structure for the $NaYF_4$:Pr NPs that is in good agreement with PXRD patterns shown in Figure 1S.

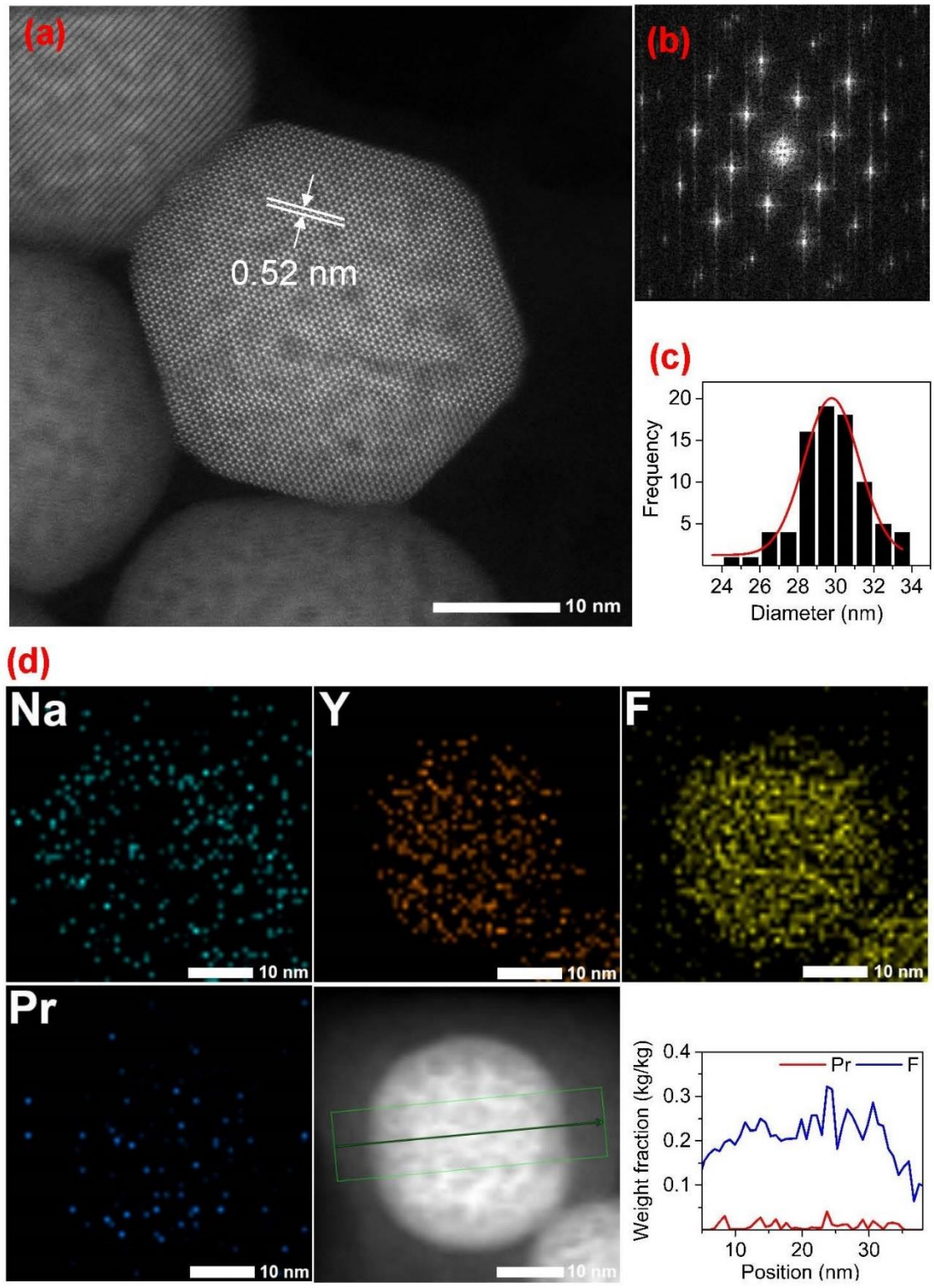

Figure 1. HRTEM image of the $NaYF_4$:Pr (1% Pr) NP sample. (a) HRTEM image with inter-planar distance of the synthesised NPs (b) SAED of synthesised NPs (c) size distribution and (d) EDX line scan across the NP sample.

Element mapping was conducted to provide insight into the distribution of Pr^{3+} within the samples. While the Pr loading is low and thus the values not quantitative, the elemental mapping of the as-synthesized NP samples, along with EDX line scan analysis across a single NP sample (Figure 1(d) and supporting information), confirms that Pr is uniformly distributed across the $NaYF_4$:Pr NP samples with minimal aggregation. The consistent PXRD patterns, particle size, particle morphology and inter-planar distances confirm that the samples have the same structure and physical characteristics across the different dopant levels.

To explore the excitation parameter space and identify new upconverting pathways, the $NaYF_4$:Pr nanoparticles were excited by scanning in both the NIR and the visible using the dual excitation system (Figure 2). The system is driven by two tuneable optical parametric oscillators (OPOs) with a pulse width of 5 ns, and repetition rate of 10 Hz. The flashlamps were synchronised by an external pulse controller such that the delay time between the laser pulses from OPO 1 and OPO 2 arriving at the sample could be independently controlled. Interference filters and beam splitting polariser cubes were used to clean up each beam line, as shown in **Figure 2**. These were needed to remove parasitic pump lines from the lasers, as well as to selectively allow the OPO idler for NIR excitation, and signal for visible excitation (see experimental section). Emission spectra were collected with a fiber coupled spectrometer at the sample.

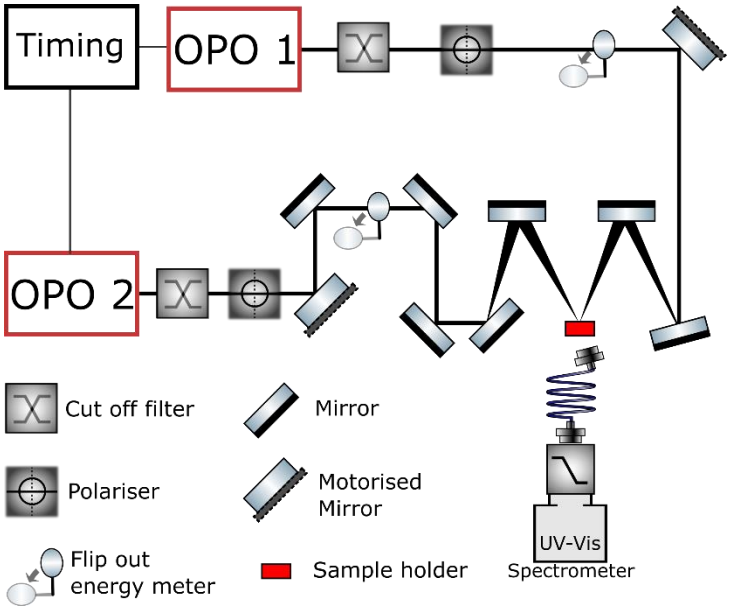

Figure 2. The dual laser setup used for the optical analysis of the rare-earth nanoparticles.

During the excitation maps, the delay between the pulse arrival time was tightly controlled and set to 10 ns peak to peak. This ensured that the pulses were not temporally overlapping at any point. This short delay time allows for the identification of sequential absorption features because as rare-earths such as praseodymium have excited state lifetimes much longer than the nanosecond regime delay time and pulse width.[16] Although kept constant, changes to the length of the excitation pulses will not result in changes to the emission spectra or upconversion pathway so long as they are considerably shorter than the lifetimes of the excited states of the ion, as then each instance of absorption can then be considered to be effectively instantaneous.

The visible wavelength excitation map for $NaYF_4$:Pr (2% Pr) in **Figure 3a** shows that upconversion emission was produced when either OPO excitation wavelength was in the range 585-590 nm. This corresponds with a Pr^{3+} absorption band promoting the $^3H_4$ --> $^1D_2$ transition. This is followed by a cooperative energy transfer process involving two Pr^{3+} ions corresponding to $^1D_2$ + $^1D_2$ --> $^3P_2$ + $^1G_4$, from which the $^3P_2$ state rapidly decays to the $^3P_{0,1}$

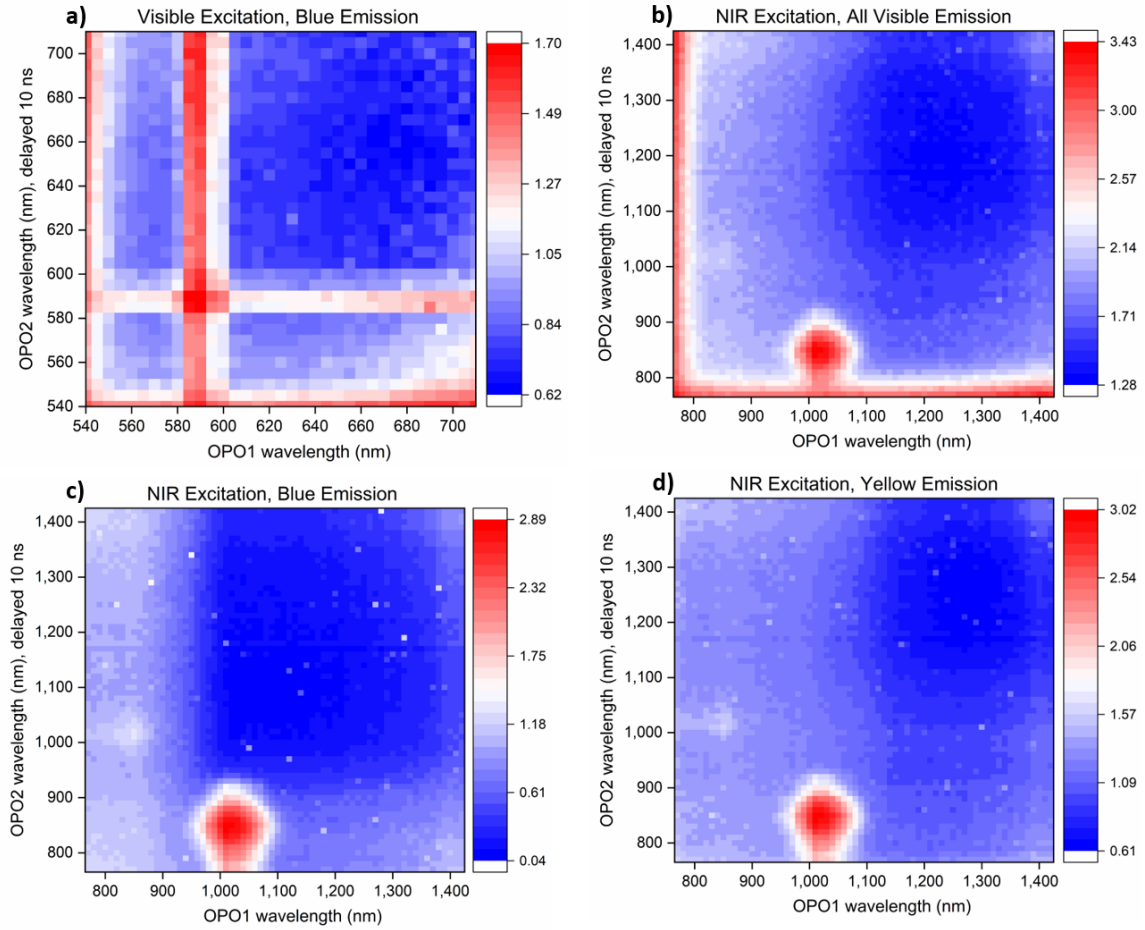

Figure 3. Excitation maps of the $NaYF_4$:Pr (2% Pr) sample. Color intensity indicates the log of emission intensity, summed over the notated range. (a) Visible Excitation scan, emission intensity summed over 450-495 nm, (b) NIR Excitation scan, emission intensity summed over 400-720 nm, (c) NIR Excitation scan, emission intensity summed over 450-500 nm (Blue) and (d) NIR Excitation scan, emission intensity summed over 600-650 nm (Yellow). We note that the bright lines at the edges of the excitation maps are due to scattered light, as the OPO source light approaches the edge of the filter's

excited states.[17] These states emit fluorescence across the visible spectrum,[17c, 18] for which the observed blue emission is anti-Stokes shifted relative to the initial excitation.

The 585-590 nm excitation could be observed through the use of only one laser source; however, the NIR excitation maps in **Figure 3b-c** show a prominent non-degenerate excitation feature, requiring both lasers to be observed. Excitation at 1020 nm followed by 850 nm leads to fluorescence at several visible wavelength bands, most prominently in the blue (490 nm) and the yellow (608 nm), which can all be assigned to emission from the $^3\mathbf{P_0}$ and $^3\mathbf{P_1}$ states.[19] This feature in the NIR corresponds to a upconversion excitation mechanism of ground state

absorption/excited state absorption (GSA/ESA) corresponding to $^3H_4$ --> $^1G_4$, $^1G_4$ --> $^3P_{0,1}$, depicted in **Figure 4a**.

Rare-earth upconversion that heavily relies on energy transfer mechanisms usually shows dramatic changes in emission intensity with changes in dopant concentration.[2, 14] To demonstrate that $NaYF_4$:Pr emission is not reliant on an ion-ion energy transfer mechanism, we additionally studied the $NaYF_4$:Pr (1% Pr) and $NaYF_4$:Pr (5% Pr) samples. The excitation maps and emission spectra were very similar for each of the Pr^{3+} doping levels synthesised (**Figure 4b**) supporting the proposed assignment of a GSA/ESA mechanism. Interestingly, minor differences were observed in the ratio of emission peaks at 490 nm and 610 nm across the differing dopant concentrations. The 5% Pr sample showed the least intense emission which may be a result of concentration quenching, as is often seen in highly doped Pr^{3+} samples.[20]

Changes in the excitation power did not change the profile of the emission spectrum for either pathway as the measured fluorescence is all being emitted from the $^3P_{0,1}$ excited states, and the fluorescence branching ratio at a given temperature is independent of state's population.[21]

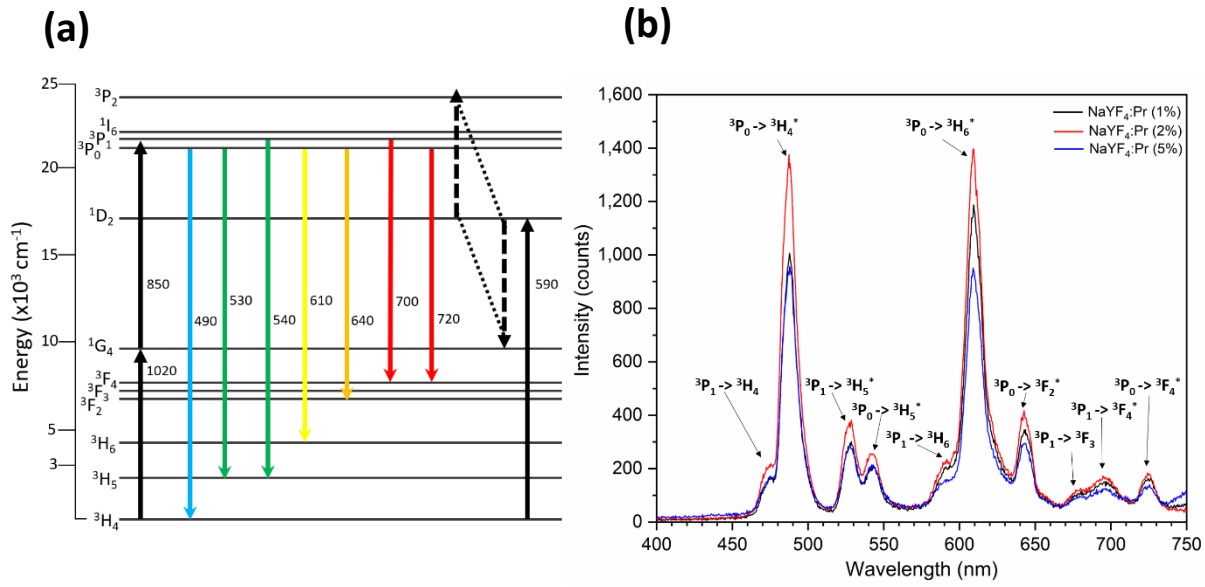

Figure 5. (a) The energy levels present in the Pr^{3+} ion. The two upconversion pathways of 1020 nm + 850 nm and 590 nm seen in the excitation maps are shown, with dashed lines representing energy transfer between neighbouring ions. Also shown are the seven most prominently observed emission bands, with approximate labels in nanometres. (b) Emission spectra from a constant mass and volume of NaYF4:Pr NP samples, after excitation with pulses of 1020 nm light followed by 850 nm light 10 nanoseconds after. Each dopant concentration responded to the excitation in a very similar way. The state transitions are labelled on the corresponding fluorescence peak, with (*) indicating the transitions depicted in Figure 3b.

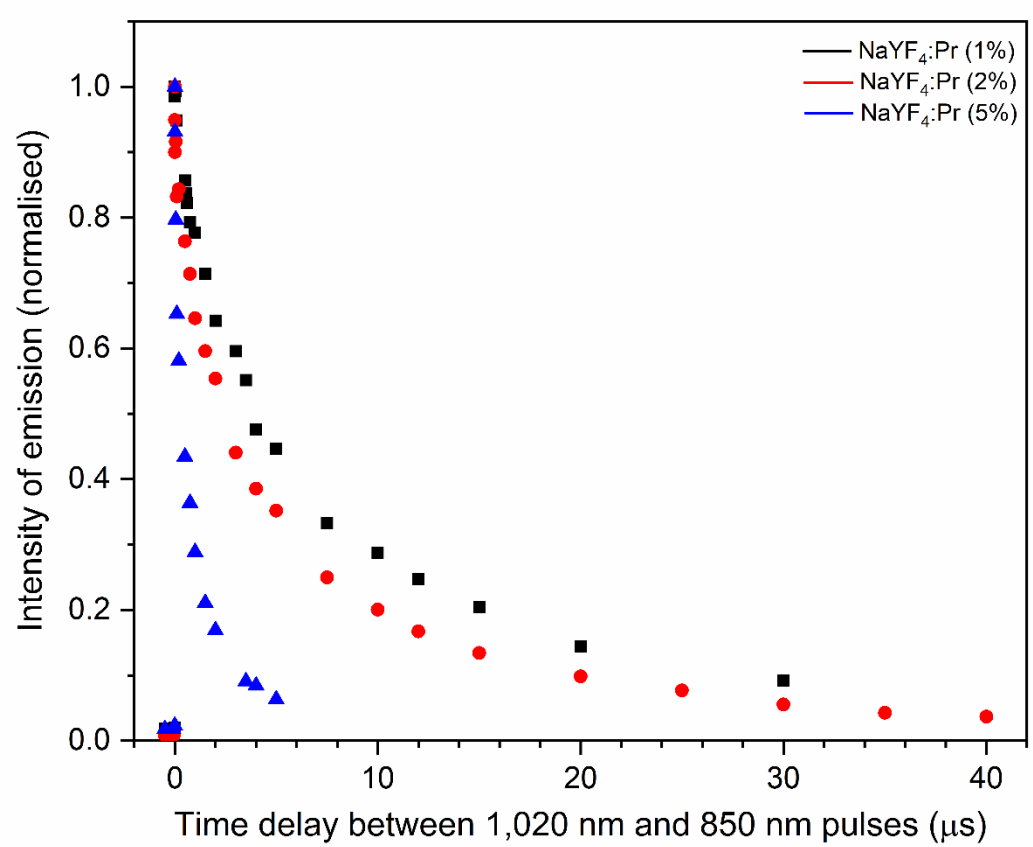

Figure 5. Decreasing luminescence intensity from the material is seen with an increase in the delay time between the GSA and ESA pulse, where a delay equalling zero indicates the 5 ns pulses arrive simultaneously. No emission is seen from any sample if the 850 nm pulse arrives first (before zero on the x-axis). Each sample's brightest emission is normalised to 1.

To further explore the dynamics of the non-degenerate upconversion fluorescence and associated energy levels, we performed excitation experiments for the combination of pump wavelengths that maximise emission from the nanoparticles where the two pulses were delayed in regards to one another. As the luminescence is due to a GSA/ESA process, no emission of light from the NaYF4:Pr NP sample is seen if the 850 nm pulse arrives first; Pr^{3+} does not have a suitable energy level that allows it to absorb this wavelength from the ground state. Furthermore, upon excitation at 1020 nm no energy transfer interactions occur between ions in the $^1G_4$ state to produce light in the visible region, emphasising the necessity of the sequential absorption of the 1020 nm then 850 nm pulses.

An artefact that can be observed in the NIR excitation maps in Figure 3 is an 'echo' of the 1020 nm and 850 nm combination, showing up at the 850 nm and 1020 nm combination where the 850 nm pulse arrives first. As stated, no emission is expected at this point as the 1020 nm pulse must arrive first in order to attain the $^1G_4$ state and for the second pulse to be absorbed. However, the system operates at 10 Hz, so while there is a delay of 10 ns between the two pulses, there is only approximately 100 milliseconds before the next pair of pulses arrive. The $^1G_4$ state is long lived enough to allow interference between the first pair of pulses and the second pair; although, many ions have decayed over this interval so only a small signal is seen.

The time resolved emission intensity depletion during the dual non-degenerate excitation at 1020 nm and 850 nm is not constant for variations in dopant concentration, despite the total luminescence being very similar. **Figure 5** shows that at higher doping concentrations, the fluorescence intensity of the material at each emission peak decays more rapidly as the delay time between the two pulses is increased. An upconversion pathway based on GSA/ESA implies that the reduction in emission intensity as the delay between the pulses is increased

depends only on the depletion of the intermediate $^1G_4$ state. Changes in the pulse delay response between dopant concentration levels therefore indicate a decrease in the observed $^1G_4$ state lifetime with increasing concentration, a trend that is seen in similar fluoride matrices, collated in **Table 1.** Due to cross relaxation energy transfer effects however the decay from this state is non-exponential at these high dopant concentrations, as has been previously observed.[22]

The dual-pump delay data does however allow for estimations of the $^1G_4$ state lifetime to be made, despite no time-resolved detection measurements being taken. The lifetime of this state is an important parameter in understanding how the material acts under dual excitation, and why the luminescence properites of the material is altered with changes in dopant concentration.

Table 1. $^1G_4$ lifetime data for Pr^{3+} ions in various matices.

Matrix	Pr^{3+} concentration [%]	$^1G_4$ lifetime [μs]	Ref.
ZBLAN[a)]	0.050	45	[22b]
ZBLAN[a)]	0.050	110	[22b]
ZBLANP[b)]	0.056	100	[14]

YBF[c)]	0.1	38	[22a]
YLF[d)]	0.24	17	[22a]
$NaYF_4$	1	13.2±1.2	This work
$NaYF_4$	2	11.9±1.6	This work
$NaYF_4$	5	1.7±0.2	This work

[a)]ZrF_4-BaF_2-LaF_3-AlF_3-NaF glass; [b)]ZrF_4-BaF_2-LaF_3-AlF_3-NaF-PbF_2 glass; [c)]barium yttrium fluoride; [d)]yttrium lithium fluoride

Despite the dual-pump delay data not conforming to a simple exponential model due to the aforementioned cross-relaxation effects, the data can be fit to a bi-exponential model corresponding to **Equation 1**:

$$Intensity = a_1 e^{-t/\tau_1} + a_2 e^{-t/\tau_2} \quad (1)$$

in which t is the time delay between pulses. The dominant factor τ_1 is the lifetime of the $^1G_4$ state and is reported in Table 1, along with the standard deviation in each fitting parameter**.** τ_2 is a minor influence to the trend, assigned to the rate at which energy is lost to different states through cross-relaxation. As the two lasers are synchronised to external timing this means that only the total intensity is required to be measured by the spectrometer, with changes in emission intensity related back to the differing pulse arrival time of the lasers.

As the material emits light in the visible region after being excited sequentially by both pulses, the emission brightness is tuneable by modifying the delay between the two pulses. Of note

is that if a delay greater than 50 microseconds is implemented, visible emission drops to negligible amounts. The delay can be modulated to increase or decrease the emission brightness, with maximum brightness achieved with the 850 nm pulse arriving 10 nanoseconds or less after the 1020 nm pulse. Importantly, a chosen brightness can be selected and reproduced, without requiring changes in excitation power. For materials that produce upconversion emission from one wavelength of light, this type of control is not possible. Even if a similar two pulse system is used, there will always be some response from the material to the first laser pulse. This is often seen in systems based on the luminescence of the 980 nm transition of the erbium ion.[23] Modulating the emission brightness of a material sensitive to a one wavelength excitation source can be achieved through changing the power density of the excitation laser.[24] However, due to the non-linear nature of upconversion, achieving and controlling both very low emission intensities as well as high brightness requires a large dynamic range in the excitation densities achievable with the laser, which is not often practical.

Praseodymium doped materials have been proposed for the application of dual laser excitation three-dimensional displays, known as two-step, two frequency (TSTF) upconversion displays.[25] To be effective in such devices, the lifetime of the intermediate excited state (in this case the $^1G_4$ state) should be selected to match the raster rate of the excitation lasers across the display. As Figure 5 demonstrates, selection of a suitable lifetime could be done through careful choice of the dopant concentration. Moreover, modulating the brightness using the delay in dual pumping, while using constant excitation, has the added advantage of preserving the spectral emission profile. This is not the case when alterating excitation power density in materials with multiple doping ions and multiple excitation pathways.[26] Fixing the pulsed laser intensity and altering delay time in the single ion doped

material allows for the emission color profile to be preserved over large changes in emission brightness.

Conclusion

$NaYF_4$:Pr nanoparticles doped with 1, 2, and 5% praseodymium ions have been synthesised and their emission/excitation properties have been mapped over a large parameter space of dual wavelength excitation combinations. This required the development of a new protocol using a custom system built around two highly tuneable OPO lasers. Doping of low amounts of rare-earths into a $NaYF_4$ matrix, without co-doping of ytterbium, is an efficient way to study their native luminescence properties. In this work nanoparticles were synthesised with consistent size, shape and controlled dopant concentration, with uniform dispersion of the Pr^{3+} observed in the particles. This allows factors such as dopant aggregation, morphology changes and surface effects to be obviated whilst altering only doping levels, an integral component of studying the fundamental optical properties of rare-earth ions. After doping of nanoparticles in this way, dual wavelength excitation maps of Pr^{3+} were produced and a non-degenerate two wavelength upconversion excitation pathway of 1020 nm and 850 nm leading to visible light emission was investigated.

Such non-degenerate two wavelength upconversion nanoparticles have interesting properties with many potential applications, such as tuneable emission brightness through changes in the dual-pump delay times. Furthermore, changes in the synthesised $NaYF_4$:Pr doping level altered how the emission brightness was depleted in response to the pulse delay, with high doping levels more rapidly reducing in emission intensity with extended delays between the dual pulses. Further work utilising this new technique is expected to enable a

better understanding of energy transfer processes in upconversion nanoparticles and the development of novel, more efficient materials for applications relying on upconversion.

Experimental Section

Synthesis of $NaYF_4$:Pr nanoparticles: $NaYF_4$:Pr nanoparticles (NPs) with 1, 2 and 5% Pr doping were prepared by thermal decomposition.[27] Specifically, 1-octadecene (ODE) was used as a solvent due to its high boiling point (315 °C), while oleic acid (OA) was used as both a solvent and surfactant to control nanoparticle growth and to prevent the aggregation of nanoparticles.[28] A full method is provided in the supporting information. This provided nanoparticle samples designated $NaYF_4$:Pr (X% Pr) based on the feed ratio of $PrCl_3$ in the reaction.

Characterization of the NPs: The as-prepared nanoparticles were characterised by powder X-ray diffraction (PXRD, structure), Transmission Electron Microscopy (TEM, particle size and morphology) and inductively-coupled plasma mass spectrometry (ICP-MS, composition). The crystal structure of the synthesized NPs was confirmed by PXRD. PXRD data for the synthesized $NaYF_4$:Pr NPs confirm all samples are crystalline. The PXRD patterns for the synthesized NP samples are presented in **Figure 1S** and show the diffraction peaks for the NPs are clearly indexed to β-$NaYF_4$ (JCPDS # 16-034). The diffraction peaks located at 17.2°, 30.1°, 30.8°, 43.5°, and 53.7° (strong diffraction peaks) correspond to the $NaYF_4$ hexagonal structure indexed with (100), (110), (101), (201), and (211), respectively (JCPDS # 16-034).

To determine if the feed ratios of Pr and Y salts used to prepare the NPs gave the expected dopant ratios, ICP-MS was used to evaluate the elemental compositions. The ICP-MS results confirmed that the molar ratio of Pr to Y in the synthesized $NaYF_4$:Pr NP samples are

approximately 1.1, 2.5 and 5.8 mole %, close to the expected values based on reactant feed ratios. The full ICP-MS results are included in the Supporting Information **Table S1**.

Optical setup of dual excitation system: Excitation of the material was achieved through two OPOTEK Radiant HE 355 LD pulsed OPO lasers. Spectral information was obtained at each wavelength combination through a fiber coupled Princeton Instruments Acton SpectraPro Sp-2300 Spectrometer with a PIXIS 100 CCD.

The light from each OPO laser was filtered through two OD9 715 nm long pass filters for the NIR excitation range, and two OD9 715 nm short pass filters for the visible light excitation range. Each laser line was additionally cleaned through a polarising beam splitting cube, before being directed by silver mirrors onto the sample. A computer-controlled motorised mirror was used in each beam line to adjust for small drifts in the beam position as the OPO laser scanned through the excitation wavelengths, allowing for the beam spot to stay on the sample.

The visible light excitation utilised a 498 nm short pass filter on the collection lens to allow for the blue emission band to be observed with the spectrometer. The NIR excitation scans utilised a 745 nm short pass filter to allow for the visible light region to be studied.

Flip out energy meters were present in each beam line, which measured the pulse energy of each laser at every excitation wavelength during the mapping procedure, averaged over 10 pulses. This allowed for the spectral data to be adjusted and normalised for changes in excitation intensity as each laser was tuned to different wavelengths. The pulse energy was between 0.5-15 mJ, see **Figure 4S and 5S**.

Acknowledgments

This research was funded by the Commonwealth Government Department of Defence, Next Generation Technologies Fund, Grand Challenge - Counter Improvised Threats (CIED) and CRC Optimising Resource Extraction(ORE) grants. The authors received funding from an Australian Government Research Training Program (RTP) scholarship, Alice Chu Postgraduate Scholarship in Chemical Engineering and the Australasian Institute of Mining and Metallurgy Education Endowment Fund (EEF) Postgraduate Research Scholarship 2020.

The authors acknowledge the instruments and scientific and technical assistance of Microscopy Australia at Adelaide Microscopy, The University of Adelaide, a facility that is funded by the University, and State and Federal Governments. The authors thank Spectragryph[29] for the Academic licence to their software, used during routine analysis.

Conflict of Interest statement

The authors report no conflicts of interest in the preceeding work.

References

[1] F. Auzel, *Chem. Rev.* **2004**, 104, 139.

[2] J. E. Moffatt, G. Tsiminis, E. Klantsataya, T. J. de Prinse, D. Ottaway, N. A. Spooner, *Appl. Spectrosc. Rev.* **2020**, 55, 327.

[3] a) D. Ma, Y. Shen, T. Su, J. Zhao, N. U. Rahman, Z. Xie, F. Shi, S. Zheng, Y. Zhang, Z. Chi, *Mater. Chem. Front.* **2019**, 3, 2058; b) A. Shalav, B. S. Richards, T. Trupke, K. W. Krämer, H. U. Güdel, *ApPhL* **2004**, 86, 013505; c) M. He, X. Pang, X. Liu, B. Jiang, Y. He, H. Snaith, Z. Lin, *Angew. Chem. Int. Ed. Engl.* **2016**, 55, 4280.

[4] a) Q. Zhan, H. Liu, B. Wang, Q. Wu, R. Pu, C. Zhou, B. Huang, X. Peng, H. Ågren, S. He, *Nat. Commun.* **2017**, 8, 1058; b) Y. Zhong, Z. Ma, F. Wang, X. Wang, Y. Yang, Y. Liu, X. Zhao, J. Li, H. Du, M. Zhang, Q. Cui, S. Zhu, Q. Sun, H. Wan, Y. Tian, Q. Liu, W. Wang, K. C. Garcia, H. Dai, *Nat. Biotechnol.* **2019**, 37, 1322; c) P. Reineck, B. C. Gibson, *Adv. Opt. Mater.* **2017**, 5, 1600446; d) Y. Liu, Y. Lu, X. Yang, X. Zheng, S. Wen, F. Wang, X. Vidal, J. Zhao, D. Liu, Z. Zhou, C. Ma, J. Zhou, J. A. Piper, P. Xi, D. Jin, *Natur* **2017**, 543, 229.

[5] a) M. Runowski, P. Woźny, I. R. Martín, V. Lavín, S. Lis, *JLum* **2019**, 214, 116571; b) C. D. S. Brites, K. Fiaczyk, J. F. C. B. Ramalho, M. Sójka, L. D. Carlos, E. Zych, *Adv. Opt. Mater.* **2018**, 6, 1701318; c) T. P. van Swieten, D. Yu, T. Yu, S. J. W. Vonk, M. Suta, Q. Zhang, A. Meijerink, F. T. Rabouw, *Adv. Opt. Mater.* **2020**, 2001518.

[6] a) F. Wang, S. Wen, H. He, B. Wang, Z. Zhou, O. Shimoni, D. Jin, *Light Sci. Appl* **2018**, 7, 18007; b) J. Zhou, Z. Liu, F. Li, *Chem. Soc. Rev.* **2012**, 41, 1323; c) Z. Yi, W. Lu, Y. Xu, J. Yang, L. Deng, C. Qian, T. Zeng, H. Wang, L. Rao, H. Liu, S. Zeng, *Biomaterials* **2014**, 35, 9689.

[7] a) X. Zhu, J. Zhang, J. Liu, Y. Zhang, *Adv. Sci.* **2019**, 6, 1901358; b) D. M. Samhadaneh, G. A. Mandl, Z. Han, M. Mahjoob, S. C. Weber, M. Tuznik, D. A. Rudko, J. A. Capobianco, U. Stochaj, *ACS Applied Bio Materials* **2020**, 3, 4358; c) S. Wen, J. Zhou, K. Zheng, A. Bednarkiewicz, X. Liu, D. Jin, *Nat. Commun.* **2018**, 9, 2415.

[8] a) A. Nadort, J. Zhao, E. M. Goldys, *Nanoscale* **2016**, 8, 13099; b) R. Reisfeld, M. Eyal, *J. Phys. Colloquiums* **1985**, 46, 349.

[9] C. Wang, X. Cheng, *J. Alloys Compd.* **2015**, 649, 196.

[10] a) K. L. Reddy, M. Rai, N. Prabhakar, R. Arppe, S. B. Rai, S. K. Singh, J. M. Rosenholm, V. Krishnan, *RSC Adv.* **2016**, 6, 53698; b) M. Liu, Y. Ye, C. Yao, W. Zhao, X. Huang, *Journal of Materials Chemistry B* **2014**, 2, 6626.

[11] a) M. S. Shariatdoust, A. L. Frencken, A. Khademi, A. Alizadehkhaledi, F. C. J. M. van Veggel, R. Gordon, *ACS Photonics* **2018**, 5, 3507; b) A. M. Kotulska, K. Prorok, A. Bednarkiewicz, *Methods Appl. Fluoresc.* **2019**, 7, 034001; c) S. Krause, M. Koerstz, R. Arppe-Tabbara, T. Soukka, T. Vosch, in *Methods Appl. Fluoresc.*, Vol. 6, 2018, 044001; d) P. Chen, M. Xu, L. Li, B. Peng, *J. Alloys Compd.* **2017**, 727, 1083.

[12] a) H. Zhang, T. Jia, L. Chen, Y. Zhang, S. Zhang, D. Feng, Z. Sun, J. Qiu, *Phys. Chem. Chem. Phys.* **2017**, 19, 17756; b) M. Ploschner, D. Denkova, S. De Camillis, M. Das, L. M. Parker, X. Zheng, Y. Lu, S. Ojosnegros, J. A. Piper, *Opt. Express* **2020**, 28, 24308; c) Z. Li, S. Xiao, X. Yang, J. W. Ding, G. Y. Tan, X. H. Yan, *PhyB* **2012**, 407, 2584.

[13] C. Jianying, P. Usha, L. Jianqiang, S. Ted, presented at Proc. SPIE 5801, Cockpit and Future Displays for Defense and Security **2005**.

[14] R. G. Smart, D. C. Hanna, A. C. Tropper, S. T. Davey, S. F. Carter, D. Szebesta, *ElL* **1991**, 27, 1307.

[15] D. Liu, X. Xu, Y. Du, X. Qin, Y. Zhang, C. Ma, S. Wen, W. Ren, E. M. Goldys, J. A. Piper, S. Dou, X. Liu, D. Jin, *Nat. Commun.* **2016**, 7, 10254.

[16] A. Vogler, H. Kunkely, *Inorg. Chim. Acta* **2006**, 359, 4130.

[17] a) R. Buisson, J.-C. Vial, *J. Physique Lett.* **1981**, 42; b) M. Kaczkan, D. A. Pawlak, S. Turczynski, M. Malinowski, *J. Alloys Compd.* **2017**, 728, 1009; c) L. E. E. de Araújo, A. S. L. Gomes, C. B. de Araújo, Y. Messaddeq, A. Florez, M. A. Aegerter, *PhRvB* **1994**, 50, 16219.

[18] a) R. Piramidowicz, R. Mahiou, P. Boutinaud, M. Malinowski, *Appl. Phys. B* **2011**, 104, 873; b) D. J. Rátiva, C. B. de Araújo, Y. Messaddeq, *JAP* **2006**, 99, 083505.

[19] a) Y. Fujimoto, J. Nakanishi, T. Yamada, O. Ishii, M. Yamazaki, *PQE* **2013**, 37, 185; b) H. Okamoto, K. Kasuga, I. Hara, Y. Kubota, *OptEx* **2009**, 17, 20227.

[20] a) J. Hölsä, T. Laamanen, T. Laihinen, M. Lastusaari, L. Pihlgren, L. C. V. Rodrigues, *OptMa* **2014**, 36, 1627; b) T. Wei, W. Bo, C. Yan, C. Yeqing, L. Jun, Z. Qingguang, *Optical Materials Express* **2019**, 9, 223.

[21] B. Walsh, N. Barnes, B. Di Bartolo, *JAP* **1998**, 83, 2772.

[22] a) C. Garapon, M. Malinowski, M. F. Joubert, A. A. Kaminskii, B. Jacquier, *J. Phys. IV* **1994**, 4, 349; b) Y. Ohishi, T. Kanamori, T. Nishi, S. Takahashi, *IPTL* **1991**, 3, 715; c) B. Jacquier, A. Remillieux, M. F. Joubert, P. Christensen, H. Poignant, *J. Non-Cryst. Solids* **1993**, 161, 241.

[23] T. Honda, T. Doumuki, A. Akella, L. Galambos, L. Hesselink, *OptL* **1998**, 23, 1108.

[24] L. X. Sun, H. Gong, B. J. Chen, H. Lin, E. Y. B. Pun, *JAP* **2009**, 105, 106109.

[25] a) E. Downing, L. Hesselink, J. Ralston, R. Macfarlane, *Sci* **1996**, 273, 1185; b) J.-H. Cho, M. Bass, H. P. Jenssen, *J. Soc. Inf. Disp.* **2007**, 15, 1029.

[26] a) C. Zhang, L. Yang, J. Zhao, B. Liu, M.-Y. Han, Z. Zhang, *Angew. Chem. Int. Ed.* **2015**, 54, 11531; b) M. Hu, D. Ma, C. Liu, J. Wang, Z. Zhang, L. Meng, *Journal of Materials Chemistry C* **2016**, 4, 6975; c) Q. Shao, G. Zhang, L. Ouyang, Y. Hu, Y. Dong, J. Jiang, *Nanoscale* **2017**, 9, 12132.

[27] X. Guo, W. Song, C. Chen, W. Di, W. Qin, *Phys. Chem. Chem. Phys.* **2013**, 15, 14681.

[28] X. Chen, D. Peng, Q. Ju, F. Wang, *Chem. Soc. Rev.* **2015**, 44, 1318.

[29] F. Menges, Spectragryph - optical spectroscopy software, http://www.effemm2.de/spectragryph/, accessed: 2020, Version 1.2.14.

Make 2020 bold in Spectragryph ref.

. Zhang, L. Yang, J. Zhao Angew. Chem. 2015, 127, 11693

(this is just editing notes for Tom for when I convert this to plain text instead of Endnote linked)